ANGULAR GYRUS RESPONSES SHOW JOINT STATISTICAL DEPENDENCE WITH BRAIN REGIONS SELECTIVE FOR DIFFERENT CATEGORIES

A PREPRINT

Mengting Fang
Department of Psychology and Neuroscience
Boston College
Boston, MA 02467
fangmg@bc.edu

Aidas Aglinskas
Department of Psychology and Neuroscience
Boston College
Boston, MA 02467
aglinska@bc.edu

Yichen Li
Department of Psychology
Harvard University
Cambridge, MA 02138
yichenli@fas.harvard.edu

Stefano Anzellotti
Department of Psychology and Neuroscience
Boston College
Boston, MA 02467
stefano.anzellotti@bc.edu

October 3, 2022

ABSTRACT

Category-selectivity is a fundamental principle of organization of perceptual brain regions. Human occipitotemporal cortex is subdivided into areas that respond preferentially to faces, bodies, artifacts, and scenes. However, observers need to combine information about objects from different categories to form a coherent understanding of the world. How is this multi-category information encoded in the brain? Studying the multivariate interactions between brain regions with fMRI and artificial neural networks, we found that the angular gyrus shows joint statistical dependence with multiple category-selective regions. Additional analyses revealed a cortical map of areas that encode information across different subsets of categories, indicating that multi-category information is not encoded in a single centralized location, but in multiple distinct brain regions.

***K*eywords** fMRI · multi-category information · multivariate statistical dependence · neural networks · angular gyrus

Introduction

A variety of cognitive tasks require integrating information about entities from different categories. Mechanisms that integrate information about people and artifacts are already at work in early stages of development: infants are more willing to help individuals who intended to give them a desirable toy over those who did not [1], and children observing repeated interactions between a person and an inanimate object infer that the person has feelings of ownership towards that object [2]. In apparent contrast with these observations, visual information about animate and inanimate entities is processed by separate, specialized brain regions [3, 4, 5, 6, 7, 8]: using functional magnetic resonance imaging (fMRI), researchers have identified regions responding selectively to faces [9, 5, 10], bodies [7, 11, 12], artifacts [13, 14] and scenes [6, 15].

Investigating the computations through which representations from different category-selective regions are integrated is challenging. Key aspects of these computations might occur at temporal and spatial scales that are beyond the resolution of noninvasive neuroimaging. However, if a brain region integrates information across multiple categories, its responses should be better predicted by the responses across multiple brain regions selective for distinct object categories, than by responses in regions that are all selective for a same category. We refer to this difference in prediction accuracy as "multi-category dependence" (MCD). Identifying regions that show multi-category dependence could serve as a stepping stone to understand integration.

Different hypotheses make distinct predictions about which brain regions might show multi-category dependence. According to the "Hub and Spokes" hypothesis [16, 17, 18], multi-category dependence should be observed in the anterior temporal lobe (ATL): a putative semantic hub integrating information in all modalities, for all semantic categories[16]. In support of this view, patients with semantic dementia – associated with neurodegeneration that affects the ATL – can present with deficits affecting multiple object categories [19]. Furthermore, transcranial magnetic stimulation (TMS) to the ATL has been reported to delay the naming of both living and nonlinving objects [20].

Other studies suggest additional regions that might show multi-category dependence. Price and colleagues [21] found that tDCS to the angular gyrus (AG) leads to faster comprehension of semantically meaningful word combinations ("tiny radish"), but not of meaningless combinations ("fast blueberry"), and proposed that this region might be involved in semantic integration. If indeed AG is broadly involved in semantic integration, we might expect its responses to show multi-category dependence as well. More recently, a study found stronger responses in the precuneus to sentences including words from multiple categories than to sentences including only words form a single category [22].

These results are not necessarily in conflict. Several processes need to combine representations across different object categories, such as the acquisition of semantic knowledge, the retrieval of episodic memory, social cognition, and decision making. Therefore, multi-category dependence might be observed in multiple regions, each specialized for a different task. In addition, distinct areas might show multi-category dependence for lexical stimuli and for visual stimuli.

While most previous studies focused on lexical stimuli, in this study we investigated multi-category dependence while participants watched quasi-naturalistic videos [23]. We used multivariate pattern dependence (MVPD, [24, 25]) based on artificial neural networks [26] to identify brain areas in which responses are better predicted by the multivariate response patterns across multiple regions that respond preferentially to different categories, than by the response patterns in regions that are all selective for a same category. In convergence with prior work using lexical stimuli [21], we found evidence for multi-category dependence in the AG. Additional tests revealed a cortical map of areas showing multi-category dependence for different subsets of categories: multi-category dependence does not occur at a single centralized location, but at multiple distinct sites.

Materials and Methods

Data

The BOLD fMRI responses (3×3×3 mm) to the movie 'Forrest Gump' were obtained from the publicly available *studyforrest* dataset (`http://studyforrest.org`). Fifteen right-handed participants took part in the study (6 females; age range 21-39 years, mean 29.4 years). The data (acquired with a T2*-weighted echo-planar imaging sequence) were collected on a whole-body 3 Tesla Philips Achieva dStream MRI scanner equipped with a 32 channel head coil. In addition to the fMRI responses to the movie, the dataset includes an independent functional localizer that was used to identify higher visual areas, such as the fusiform face area (FFA), the extrastriate body area (EBA), and the parahippocampal place area (PPA). See [23] for more details.

During the category localizer, participants were shown 24 unique gray-scale images from each of six stimulus categories: human faces, human bodies without heads, small artifacts, houses, outdoor scenes, and phase scrambled images. They

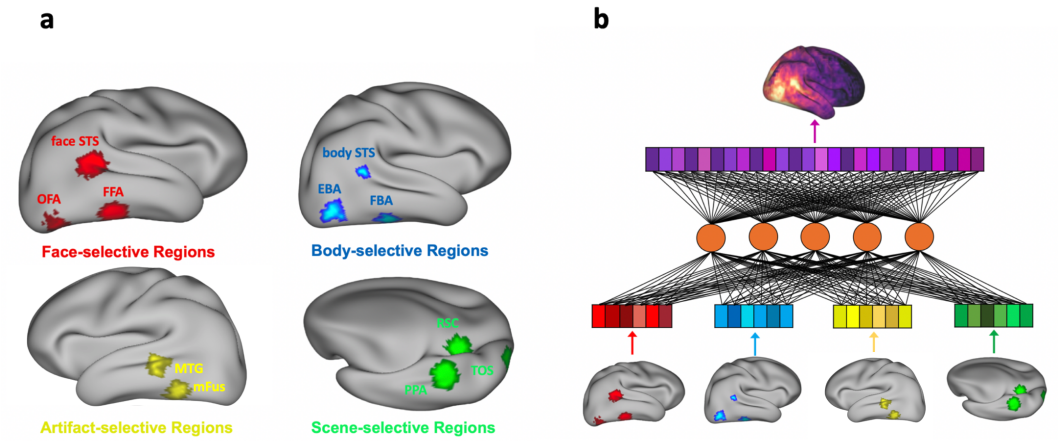

Figure 1: **a.** Category-selective ROIs of one example participant shown on an inflated cortical surface. Face-selective regions are shown in red (OFA, FFA, and face STS). Body-selective regions are shown in blue (EBA, FBA, and body STS). Artifact-selective regions are shown in yellow (mFus and MTG). Scene-selective regions are shown in green (TOS, PPA, and RSC). **b.** Illustration of an artificial neural network using the response patterns from all category-selective regions combined as input to predict neural activities across the whole brain. The hidden layer is displayed with five nodes for visualization purposes, whereas the networks used for the analyses in this article have hidden layers with 100 nodes.

were presented with four block-design runs and a one-back matching task. Then, to collect fMRI responses to the movie, the movie stimulus 'Forrest Gump' was cut into eight segments, approximately 15 min long each. All eight movie segments were presented individually to participants in chronological order in 8 separate functional runs.

Preprocessing

Data were first preprocessed using fMRIPrep (`https://fmriprep.readthedocs.io/en/latest/index.html`), which is a robust and convenient pipline for preprocessing of diverse fMRI data. Anatomical images were skull-stripped with ANTs (`http://stnava.github.io/ANTs/`), and FSL FAST was used for tissue segmentation. Functional images were corrected for head movement with FSL MCFLIRT (`https://fsl.fmrib.ox.ac.uk/fsl/fslwiki/MCFLIRT`), and were subsequently coregistered to their anatomical scan with FSL FLIRT. The raw data of one participant could not pass the fMRIPrep processing pipeline. For the remaining 14 subjects, we denoised the data with CompCor [27] using 5 principal components extracted from the union of cerebrospinal fluid and white matter.

ROI definition

Four sets of category-selective brain regions were identified using the first block-design run in the category localizer session (Fig. 1a): face-selective regions (occipital face area - OFA, fusiform face area - FFA, and face-selective posterior superior temporal sulcus - face STS), body-selective regions (extrastriate body area - EBA, fusiform body area - FBA, and body-selective posterior superior temporal sulcus - body STS), artifact-selective regions (medial fusiform gyrus - mFus and middle temporal gyrus - MTG), and scene-selective regions (transverse occipital sulcus - TOS, parahippocampal place area - PPA, and retrosplenial cortex - RSC). Data were modelled with a standard GLM using FSL FEAT [28], and each seed ROI was defined as a 9mm radius sphere centered in the peak for its corresponding contrast (e.g. face-selective contrast: faces $>$ bodies, artifacts, scenes, and scrambled images). We combined data from both left and right hemisphere for each ROI and then selected the 80 voxels which showed the highest t-values for the contrast between the preferred category and other categories. Finally, the face-, body-, scene-selective regions were identified with 240 voxels each, and the artifact-selective regions consist of 160 voxels.

Additionally, we created a group-average gray matter mask using the gray matter probability maps generated during preprocessing, with a total of 53539 voxels. This mask was used as the target of prediction ROI in the multivariate pattern dependence analyses (see below).

MVPN: Multivariate pattern dependence network

Most research on the interactions between brain regions has focused on the mean responses across voxels in different regions. However, fine grained patterns of response encode important information that could be lost by spatial-averaging. Over the past two decades, multivariate pattern analysis (MVPA, [29, 30]) of fMRI data has led to progress in the investigation of neural coding at a level of specificity that could not be achieved with univariate analyses [31, 32, 33, 34, 35]. Despite this, relatively few attempts have been made to leverage the potential of multivariate analyses to study brain connectivity (see [25] for a recent review). A recent study [24] has developed a technique that investigates the interactions between brain regions in terms of the multivariate relationship between their response patterns (multivariate pattern dependence - MVPD). MVPD has been shown to offer greater sensitivity than univariate connectivity methods [24], and uses independent training and testing data, thus offering improved robustness to noise.

The original MVPD formulation [24] used principal component analysis (PCA) to reduce the dimensionality of fMRI response patterns, and subsequently used linear regression as a model of the statistical dependence between brain regions. A more recent version of MVPD used simple artificial neural networks [36], but was limited to a small number of nodes in the hidden layer, and still relied on PCA for dimensionality reduction. Artificial neural networks can themselves perform dimensionality reduction if needed [37]. In addition, using state-of-the-art software packages for artificial neural networks paves the way for the training of more complex network architectures thanks to the use of general purpose graphic processing units (GPGPUs).

To take advantage of these benefits, in this work we extended MVPD to larger artificial neural networks (multivariate pattern dependence network, or MVPN), and we implemented it in PyTorch to train the networks on four Tesla V100 GPUs. The networks received as inputs multivariate patterns of response in one or more sets of category-selective regions, and were trained to predict the patterns of response in the whole brain.

More formally, let's consider an fMRI scan with m experimental runs. We denote the multivariate timecourses in the predictor region by $X_1, ..., X_m$. Each matrix X_i is of size $n_X \times T_i$, where n_X is the number of voxels in the predictor region, and T_i is the number of timepoints in the experimental run i. Analogously, $Y_1, ..., Y_m$ denote the multivariate timecourses in the region that is the target of prediction, where each matrix Y_i is of size $n_Y \times T_i$, and n_Y is the number of voxels in the target region.

MVPN was trained with a leave-one-run-out procedure to learn a function f such that

$$Y_{train} = f(X_{train}) + E_{train},$$

where X_{train} and Y_{train} denote data in the predictor region and data in the target region respectively during the training runs. E_{train} is the error term. Specifically, for each choice of an experimental run i, data in the remaining runs were concatenated as the training set

$$D_{\setminus i} = \{(X_1, Y_1), ..., (X_{i-1}, Y_{i-1}), (X_{i+1}, Y_{i+1}), ..., (X_m, Y_m)\},$$

while data $D_i = \{(X_i, Y_i)\}$ in the left-out run i were used as a testing set.

As a measurement of the multivariate statistical dependence, we calculated the proportion of variance explained between the predictor region and every other voxel in a group-level gray matter mask created from the gray matter probability maps generated during preprocessing. For each voxel j in the target region, variance explained in run i was calculated as

$$\mathrm{varExpl}_i(j) = max\left\{0, 1 - \frac{var(Y_i(j) - f_j(X_i))}{var(Y_i(j))}\right\},$$

where X_i is the timecourse in the predictor region for run i, and $f_j(X_i)$ is the prediction by MVPN for voxel j. The values $\mathrm{varExpl}_i(j)$ obtained for the different runs $i = 1, ..., m$ were averaged, yielding $\overline{\mathrm{varExpl}}(j)$.

Exploring multi-category dependence sites

To identify brain regions with multi-category dependence, we used the 8 experimental runs during which participants watched the movie 'Forrest Gump'. The runs were used as separate folds for cross validation. In a first analysis, we used MVPN to calculate the variance explained in each gray matter voxel using each of the four category-selective regions (face, body, artifact, and scene) individually. In a second analysis, we combined all category-selective regions jointly as inputs of MVPN to predict the fMRI responses of each voxel in the gray matter mask.

If a target region only encodes information from one category of objects, using the responses from regions selective for multiple categories as predictors should not improve over using only the responses in the regions from the one category yielding the best predictions. Instead, if the responses in a target brain region are predicted significantly better by a

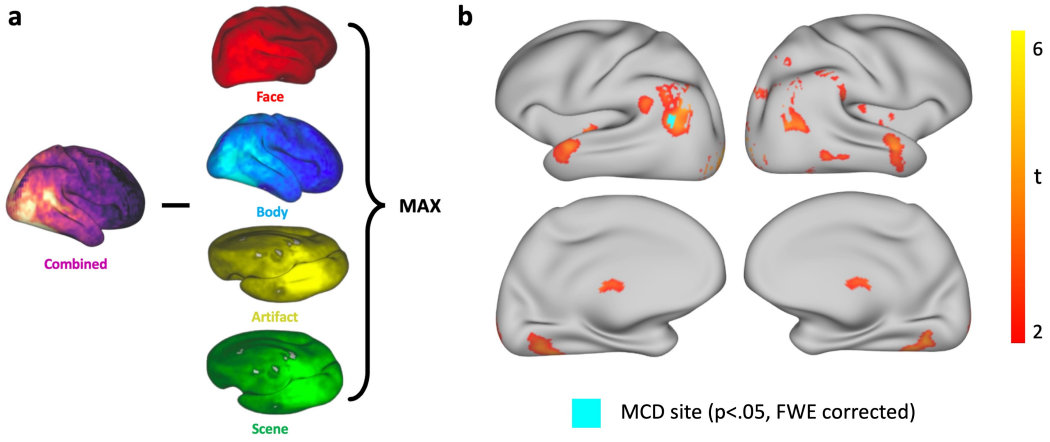

Figure 2: **a.** The MVPN combined-minus-max approach to detect multi-category dependence (MCD) sites jointly encoding information from multiple category-selective regions. **b.** Statistical t-maps of the 5-Layer Dense MVPN model computed from Δ varExpl across subjects. Δ varExpl is the voxelwise difference between the variance explained predicted by the combined model using the response patterns from all category-selective regions as input, and the variance explained predicted by the model using the response patterns from regions selective for the single best-predicting category as input. The SnPM threshold corrected at $p < 0.05$ FWE is 5.11. T-maps are thresholded within the range [2,6] for visualization purposes. The identified MCD site within left AG is shown in aqua color.

model including all category-selective regions combined, than by the best of the category-selective regions in isolation, we can conclude that multiple category-selective regions have unique contributions to the overall statistical dependence with that target region. We refer to this approach as the "combined-minus-max" approach.

To make things more precise, for each voxel j we can denote with $\mathrm{varExpl}_{all}(j)$ the variance explained by MVPN using as input the responses in all category-selective regions (Fig. 1b), and with $\mathrm{varExpl}_{max}(j)$ the variance explained by MVPN using as input the responses in regions corresponding to the single best-predicting category. We then calculated for each voxel the difference

$$\Delta\,\mathrm{varExpl}(j) = \mathrm{varExpl}_{all}(j) - \mathrm{varExpl}_{max}(j),$$

and used it as a metric to evaluate whether a voxel exhibits multi-category dependence by jointly encoding information across multiple regions selective for different categories. For each subject, we calculated the difference Δ varExpl for each voxel in the gray matter mask, and we computed statistical significance across participants with statistical non-parametric mapping using the SnPM extension for SPM (`http://warwick.ac.uk/snpm`), obtaining pseudo-t statistics. Regions consisting of voxels with statistically significant pseudo-t-values were defined as candidate multi-category dependence (MCD) sites.

Using the combined-minus-max approach alone, however, we can not rule out the possibility that the better predictive accuracy of the combined MVPN model in candidate MCD sites is simply due to the increased number of voxels: control analyses are needed. To test whether combined-minus-max effects are driven by differences in the number of voxels, we further conducted a control analysis using voxels extracted from primary visual cortex (V1) as predictors. In this analysis, we randomly selected four non-overlapping groups of voxels in V1, such that these groups have the same number of voxels as our four sets of category-selective regions. We then used responses from these groups of voxels in V1 to run a control analysis matched in the number of voxels to the original combined-minus-max analysis. Specifically, we ran MVPN analyses using as inputs the responses from each of the four V1 groups in isolation, and then using responses in all groups combined. Next, we performed a combined-minus-max analysis and computed the statistical significance of Δ varExpl across participants. If a region we previously identified as a MCD site also shows statistical significance in the control analysis, the observed results might be driven by the number of voxels rather than by multi-category dependence, and therefore the region is removed from the set of candidate MCD sites.

It is important to note that there is some overlap between adjacent category-selective ROIs (e.g. face-selective FFA and body-selective FBA), indeed this overlap has been reported in several previous studies [38, 12]. However, the overlap actually makes our analysis more stringent when seeking for MCD sites. Suppose that one voxel in the face-selective ROI overlaps with the body-selective ROI and encodes information about both face and body, a region jointly encoding information about face and body might not survive our combined-minus-max analysis and could not be detected (because the face-selective ROIs could be selected as the max, and would include information about both faces and

bodies). The more voxels with overlapping category-selectivity, the harder it would be to find MCD sites. In contrast, the non-overlapping selection of the control V1 voxels makes it easier to find regions showing combined-minus-max effects in the control analysis, thus excluding voxels showing significant results in the control analysis further increases the rigor of our findings.

Neural network architectures

To make sure that the results do not depend on choosing a very specific neural network architecture, we trained MVPN using three different neural network architectures (Supplementary Fig. S1a), and identified regions that showed significant effects in the combined-minus-max analysis in all architectures. All network architectures were linear, because previous studies did not find an advantage for using nonlinear neural networks in MVPD [39]. All architectures used 100 hidden nodes in each hidden layer. The first architecture was a one-layer feedforward network (Supplementary Fig. S1a, left). Since previous studies have shown that deeper networks can approximate the same classes of functions as shallower networks using fewer parameters [40], we then tested a second, deeper architecture: a five-layer feedforward network (Supplementary Fig. S1a, middle). Finally, a challenge encountered in training deep neural networks is the vanishing-gradient problem [41]: as the gradient of the loss function is back-propagated across multiple layers, the weight updates can become progressively smaller, affecting learning in early layers of the network. For this reason, we also tested a five-layer DenseNet [42]. The DenseNet architecture includes connections that bypass multiple layers (Supplementary Fig. S1a, right), enabling more direct backpropagation of the loss function to early layers.

All architectures were trained over 5000 epochs using stochastic gradient descent (SGD) on a mean squared error (MSE) loss, with a learning rate of 0.001 and a momentum of 0.9. We used a batch size of 32, and batch normalization was applied to the inputs of each layer. The original code implemented in PyTorch is available at https://github.com/sccnlab/PyMVPD. More details are provided in the PyMVPD toolbox [26].

Pairwise and three-way MCD analysis

Multi-category dependence might not only occur across all four object categories. Instead, it is possible to find MCD effects in other brain areas when considering a pair or a triplet of category-selective regions. To investigate multi-category dependence in more depth, we implemented the combined-minus-max approach on different pairs and triplets of categories, and conducted the following pairwise and three-way MCD analysis.

In the pairwise MCD analysis, we used responses in each pair of category-selective regions (face and body, face and artifact, face and scene, body and artifact, body and scene, artifact and scene) as MVPN inputs to calculate the variance explained in each gray matter voxel. We then calculated $\Delta\,\mathrm{varExpl}_{pair}$ for each voxel by subtracting the variance explained predicted by responses in one pair of category-selective regions from the variance explained predicted by responses in regions selective for the better-predicting category within that pair. We used the average $\Delta\,\mathrm{varExpl}_{pair}$ across different runs as a metric to identify candidate brain areas that jointly encode information from two category-selective regions in each pair. A control analysis was then performed following the same approach described previously (in the "Exploring multi-category dependence sites" section): we repeated the combined-minus-max analysis with randomly selected subsets of V1 voxels to exclude regions that were simply better predicted by the combined model due to the greater number of voxels.

In the three-way MCD analysis, responses in each triplet of category-selective regions (face and body and artifact, face and body and scene, face and artifact and scene, body and artifact and scene) were used as inputs to our MVPN model. The $\Delta\,\mathrm{varExpl}_{triplet}$ for each voxel was calculated by subtracting the variance explained predicted by responses in one triplet of category-selective regions from the variance explained predicted by responses in regions selective for the best-predicting category within that triplet. We took the average $\Delta\,\mathrm{varExpl}_{triplet}$ across runs as a metric to identify candidate areas that jointly encode information from three category-selective regions in each triplet. Finally, a control analysis was performed (following the approach described above) to rule out voxel-driven regions that did not contribute to the three-way multi-category dependence.

Representational similarity analysis

We used representational similarity analysis (RSA) [43, 44] to study the representational geometry of MCD sites and to investigate how they differ from the representational geometry in category-selective regions. RSA is a multivariate method that calculates the pairwise dissimilarities between multivariate activation patterns in a brain region, yielding a representational dissimilarity matrix (RDM). In this study, we used the correlation distance (one minus the Pearson correlation) as dissimilarity metric. Before calculating the correlation distance, for each subject the average response pattern across all categories was subtracted from the data [45].

Since we used the first run of the category localizer to identify category-selective ROIs, we used the remaining three runs of the localizer for the following analyses. For each of the four sets of category-selective ROIs, response patterns in each of the regions in the set were concatenated, yielding four RDMs for each of the 14 participants. For each of the candidate MCD sites, we first defined a 9mm radius sphere (123 voxels) centered in the peak of its SnPM t contrast map obtained from the combined-minus-max analysis using the best-performing MVPN model (i.e. 5-Layer Dense MVPN). Next, we selected 50 voxels with the highest t values for each candidate MCD site and calculated the RDMs on the new set of voxels. RDMs were then averaged across participants, and the standard error of the mean (SEM) was calculated as a measure of the intersubject variability of correlation distance for each pair of stimuli. We used radar charts to visualize the within-region and between-region differences in dissimilarity. Note that because RDMs are symmetric about a diagonal of zeros, we only extracted the upper (or equivalently the lower) triangle of the matrices for radar chart visualization.

Results

Identification of MCD sites

To identify candidate sites that jointly encode information from regions selective for different object categories, we calculated a multi-category dependence (MCD) index for each voxel in the brain (mathematical details are reported in the Materials and Methods section). The index was computed as the difference between the proportion of variance explained by a model using all category-selective regions as predictors (henceforth the 'combined model'), and the proportion of variance explained by a model using regions selective for the single best predicting category as predictor (henceforth, the 'max model', Fig. 2a). To ensure the robustness of the results across different neural network architectures, we computed this index using 1-Layer, 5-Layer, and 5-Layer Dense MVPN architectures (Supplementary Fig. S1a). The results showed that the 5-Layer Dense network outperformed the 1-Layer network and the 5-Layer network without dense connections in terms of the combined variance explained in each candidate MCD site (Supplementary Fig. S1b). For each neural network architecture, we used a group-level analysis to identify voxels in which the MCD index was significantly greater than zero ($p < 0.05$ corrected with SnPM). Then, we selected voxels where the MCD index was significantly greater than zero for all three network architectures as candidate sites for multi-category dependence.

The nature of this analysis is such that the number of voxels used as predictors in the combined model is greater than the number of voxels used as predictors in the max models. Therefore, we performed a control analysis using the best-predicting 5-Layer Dense MVPN model to rule out the possibility that positive values of the MCD index might be driven by differences in the number of input voxels. In the control analysis, we repeated the same procedure we used to identify candidate sites for multi-category dependence, but we replaced the category-selective regions with control subregions consisting of voxels randomly sampled from primary visual cortex (V1). Importantly, the control subregions were matched in number of voxels to the category-selective regions. To make the control more stringent, we adopted a less conservative threshold for the MCD index. Specifically, we identified voxels whose pseudo-t-values (computed with a nonparametric test using SnPM) in the control analysis were significantly greater than zero without applying multiple comparison correction (pseudo-t(13) = 1.77, P < 0.05, one-sided); any MCD effects in these voxels were discarded as possible artifacts of the number of voxels.

In a region within left AG (Fig. 2b, peak MNI coordinates: -57, -69, 21), the MCD index was significantly greater than zero for all neural network architectures tested (lowest pseudo-t(13) = 5.20, p < 0.05). At the same time, this region did not show significant effects in the control analysis (indeed, in this region all t-values in the control analysis were negative: highest pseudo-t(13) = -1.27, see Table 1 for a complete report of the pseudo-t-values for all voxels). The location of this region within angular gyrus was confirmed with Neurosynth [46]. The angular gyrus has been previously found to integrate information across multiple sensory modalities [47], our results indicate that it also jointly encodes information across multiple object categories. Three other regions (two in the vermis, one in occipital gyrus) showed significant effects in the MCD analysis, but also in the control analysis, thus they were removed from subsequent analyses (see Table 1 for details).

Representational geometry of the MCD site: AG

Having identified a MCD site in the left AG, we asked whether this region inherits its representational similarity structure from category-selective regions, showing more similar responses to pairs of objects that are both animate or both inanimate. To address this question, we used response patterns to different object categories during the functional localizer to calculate representational dissimilarity matrices (RDMs, [43]) for the MCD site and for each set of category-selective regions (Fig.3).

Table 1: **Candidate MCD sites that jointly encode information across all four category-selective ROIs.** We selected candidate MCD sites from brain regions with significant t-values ($p < 0.05$, FWE-corrected) computed from the combine-minus-max analysis across all three network architectures: 1-Layer MVPN, 5-Layer MVPN, and 5-Layer Dense MVPN. The location of each site is expressed in MNI coordinates. For each voxel in the candidate MCD sites, we also computed the corresponding t value in the control analysis using the best-performing 5-Layer Dense MVPN. # vox indicates the total number of voxels in each site.

Candidate MCD Sites	MNI Coordinates	5-Layer Dense	1-Layer	5-Layer	Control	# vox
		t	t	t	t	
Angular Gyrus	(-57,-69,21)	5.72	7.51	6.57	-1.27	8
	(-57,-69,24)	5.20	7.30	6.81	-1.81	
	(-57,-66,18)	5.28	6.07	5.25	-1.69	
	(-57,-66,21)	5.53	7.16	6.09	-2.86	
	(-54,-72,21)	5.58	7.69	6.48	-1.62	
	(-54,-69,21)	5.61	8.03	7.31	-2.54	
	(-54,-69,24)	5.30	8.24	8.06	-2.79	
	(-54,-66,24)	5.16	7.81	7.17	-3.68	
Vermis 1	(-3,-75,-9)	5.37	7.98	7.98	5.59	7
	(-3,-72,-12)	5.41	7.43	6.36	3.67	
	(-3,-72,-5)	5.85	8.07	7.75	5.97	
	(-3,-69,-5)	5.40	7.89	6.59	5.40	
	(0,-75,-12)	5.26	7.85	7.30	5.11	
	(0,-75,-9)	5.52	8.18	8.19	5.76	
	(0,-72,-12)	5.72	7.90	6.64	3.86	
Vermis 2	(3,-72,-5)	5.11	7.17	6.15	5.11	1
Occipital Gyrus	(24,-102,8)	5.26	6.14	5.35	3.83	4
	(24,-99,8)	5.47	7.46	6.64	3.75	
	(24,-99,11)	5.52	6.89	6.33	3.90	
	(27,-99,8)	5.62	6.85	6.05	3.49	

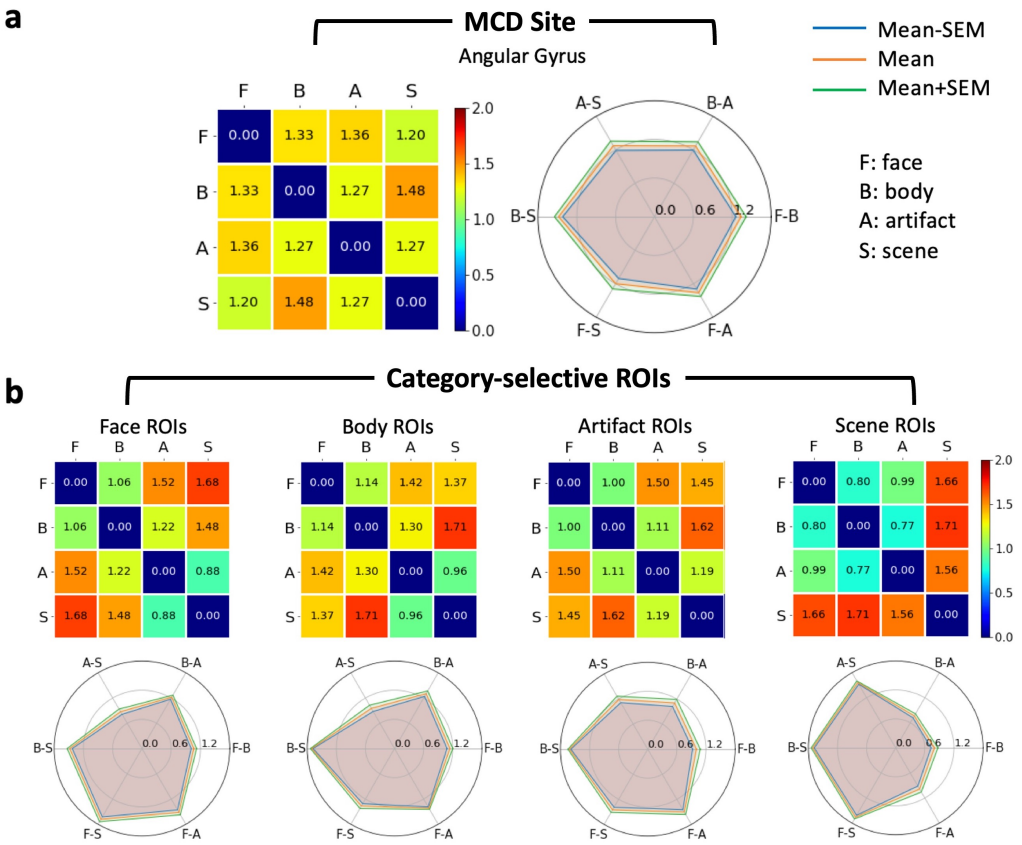

Figure 3: **Using representational dissimilarity matrices (RDMs) and radar charts to discriminate between MCD site and category-selective ROIs. a.** RDMs (top) and radar charts (bottom) for average brain activities across subjects in the MCD site: the left angular gyrus; **b.** RDMs (top) and radar charts (bottom) for average brain activities across subjects in four category-selective ROIs: face-selective ROIs, body-selective ROIs, artifact-selective ROIs, and scene-selective ROIs. In each radar chart, the middle boundary represents the average representational dissimilarity across subjects, the inner boundary represents the average representational dissimilarity minus the standard error of the mean (SEM), and the outer boundary represents the average representational dissimilarity plus SEM.

First, we replicated the finding that representations in inferior temporal cortex are organized by animacy [48, 49]. We found that in face-, body- and artifact-selective ROIs, object pairs that were both animate (faces and bodies) or both inanimate (artifacts and scenes) elicited more similar responses than object pairs with different animacy (faces and scenes, faces and artifacts, or bodies and scenes) - Fig. 3b. This similarity structure leads to asymmetrical radar charts for the category-selective ROIs (Fig. 3b). In scene-selective ROIs, response patterns to scenes showed high dissimilarity from the responses to all other object categories, while the dissimilarty between pairs of non-scene categories was low (Fig. 3b). However, these effects were not observed in the left AG MCD site (Fig. 3a). By contrast, in the MCD site all pairs of categories showed comparable dissimilarity (Fig. 3a).

Pairwise and three-way MCD

Combining information about faces and bodies could facilitate the recognition of individuals and their actions, while combining information about artifacts and scenes could help to search for objects in their habitual contexts. Several distinct cortical sites might encode information about multiple object categories jointly, in the service of distinct cognitive functions. Can we identify brain regions that show multi-category dependence for specific subsets of categories? To address this question systematically, we calculated the MCD index for all pairs and triplets of categories. The resulting SnPM pseudo-t contrast maps were thresholded at $p < 0.05$ (FWE corrected). For each pair and triplet of categories, we also ran control analyses using subregions of V1 matched in terms of the number of voxels, following the same procedure we used in the analysis with all four categories (see Materials and Methods for details).

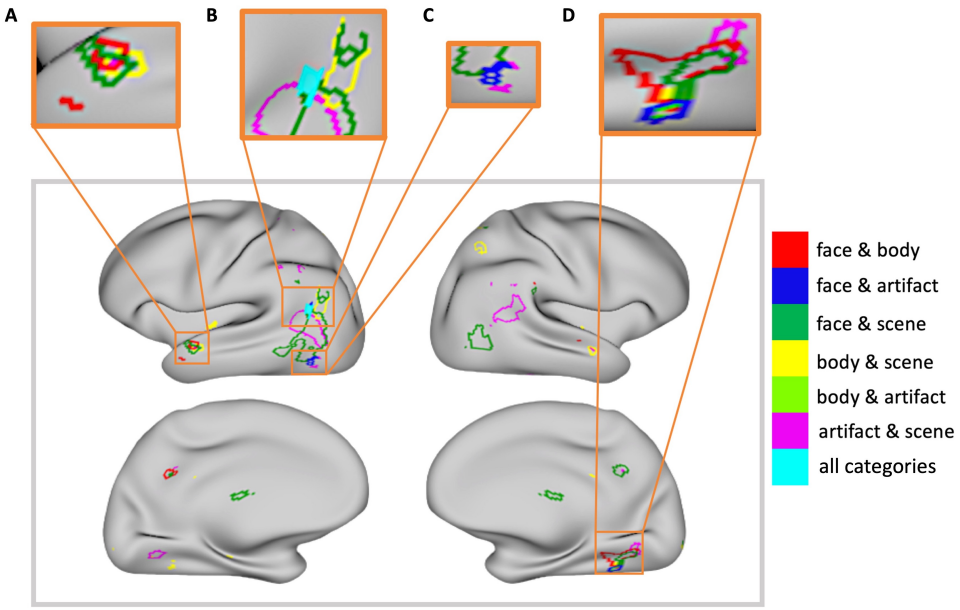

Figure 4: **Cortical map of pairwise MCD.** The outlines of brain areas with significant pairwise MCD effects ($p < 0.05$, FWE corrected) but not in the control analysis ($p < 0.05$, uncorrected) are colored in red (face & body), blue (face & artifact), green (face & scene), yellow (body & scene), lime (body & artifact), and purple (artifact & scene). The left AG MCD site identified across all four categories is shown in aqua color. The four orange boxes on the top panel depicted the enlarged patterns of pairwise MCD in the dorsal ATL, the AG, left MTG, and the ventral occipitotemporal cortex.

We plotted the outlines of sites showing significant MCD of pairs of categories on an inflated cortical surface (Fig. 4). This analysis revealed that the left AG MCD site identified in the first portion of this study is surrounded by a cortical map of regions showing significant pairwise MCD for different pairs of categories. More precisely, this cortical map is constituted by regions showing MCD effects between scenes and each of the other three categories separately, demonstrating joint encoding of responses to entities and to the environments in which they are embedded (Fig. 4; face and scene, in green; body and scene, in yellow; artifact and scene, in purple).

In addition to this cortical map of multi-category dependence in the left AG, the analysis revealed other cortical areas displaying evidence for MCD between pairs of categories (a magnified view of these areas is shown on the top panel of Fig. 4). First, a region in dorsal ATL showed evidence of overlapping face-body, face-scene, and body-scene MCD (shown in the leftmost magnification box, Fig. 4). Second, pairwise MCD effects were observed in the left middle temporal gyrus (MTG, shown in the third magnification box from the left, Fig. 4). Lastly, pairwise MCD effects of responses selective for faces and bodies, faces and artifacts, faces and scenes, and bodies and scenes were observed in a portion of the ventral occipitotemporal cortex (shown in the fourth magnification box from the left, Fig. 4). Overlap between face-body and face-scene MCD effects was observed in the precuneus (Fig. 4). Overall, MCD effects showed a substantial degree of bilateral symmetry.

Consistent with the overlap in pairwise multi-category dependence results, we also found significant three-way MCD effects in ATL, middle temporal gyrus, and ventral occipitotemporal cortex (Fig. 5a). To quantify the contribution of different categories to predicting responses in these regions, we computed the variance explained by the best-predicting 5-Layer Dense MVPN model using all combinations of individual, pairwise, and three-way sets of categories (Fig. 5b-f). Together, these results show that in addition to the MCD site in angular gyrus, pairwise and three-way MCD effects can be observed at multiple other sites, including ATL and MTG.

Discussion

This study aimed to identify cortical sites that jointly encode responses across multiple category-selective brain regions. Using multivariate analyses of the interactions between brain regions, we identified a multi-category dependence (MCD) site in the left angular gyrus (AG), surrounded by a cortical map of regions showing pairwise and three-way MCD effects. Combining information from multiple object categories is needed for a variety of cognitive functions - what might be the functional role of the multi-category representations we identified in AG? The AG is a multimodal integration area

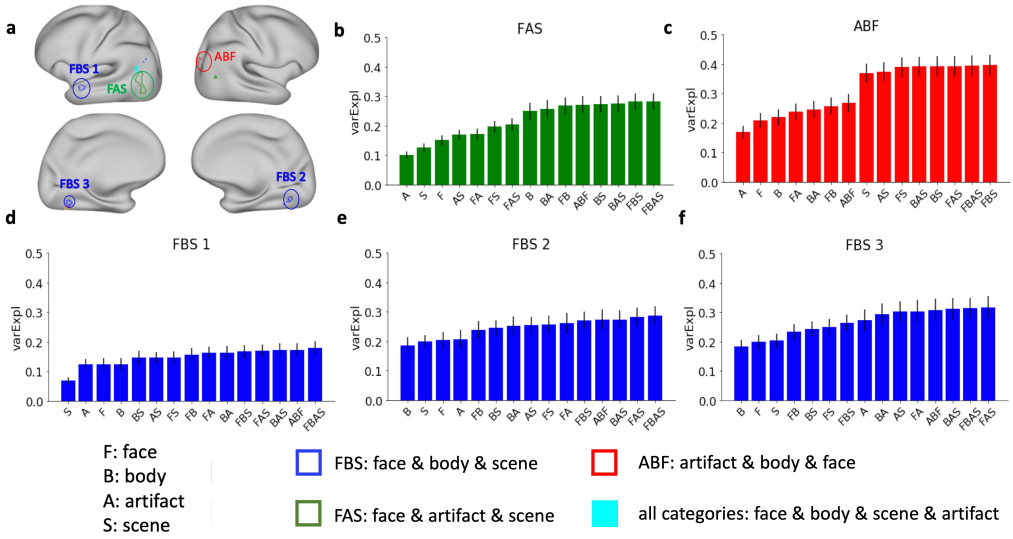

Figure 5: **a.** Cortical sites showing three-way multi-category dependence. **b-f.** Predictive accuracy across three-way MCD regions using response patterns from different sets of category-selective regions as inputs (e.g. F: face-selective regions, FB: face- and body-selective regions, ABF: artifact-, body-, and face-selective regions) with the 5-Layer Dense MVPN model. Error bars indicate the standard error of the mean (SEM).

[47] that has been implicated in a variety of cognitive processes. Specifically, the AG has been implicated in semantic memory [50, 51], episodic memory [52, 53], and bottom-up attention [54]. More recently, it has been proposed that AG might play a key role for the representation of event semantics [55] and schemas [56], and that it might serve as a temporary buffer that integrates spatiotemporal information [57].

Previous studies reported evidence of a role of AG in combinatorial semantics, showing that AG responds more to meaningful word combinations than to non-meaningful ones, and that the degree of atrophy in AG is inversely related to combinatorial performance in patients with semantic dementia [58]. In addition, transcranial direct current stimulation (TDCS) of the left AG selectively affects the speed of comprehension of semantically meaningful word combinations [21]. These observations are consistent with the sensitivity of AG to combinatorial spatial and non-spatial patterns [56]. AG was also found to respond differentially during the integration of multiple cues when making judgments about ambiguous words [59], even when the cues were from different categories (facial expressions and locations). Our results directly demonstrate the statistical dependence of AG responses on responses across regions selective for multiple different categories during the observation of complex, quasi-naturalistic videos (Fig. 2b).

In addition, the results reveal a cortical map of regions in and around AG whose responses depend on different pairs of category-selective networks (Fig. 4). This cortical map is characterized by regions jointly encoding scene-selective responses with responses selective for one other category (scenes and artifacts, scenes and bodies, scenes and faces), suggesting that AG might integrate objects and their scene contexts to represent complex situations and events. This proposal is consistent with the hypothesis that AG might be involved in event representations [55], and that it might serve as a temporary buffer [57], as the locations and interactions of multiple objects and their functional significance within an event (i.e. whether they play a causal role) can vary from situation to situation.

Besides the AG, the ATL has been implicated in the integration of information across multiple modalities and categories [16]. In addition, multivariate analyses of fMRI data suggest that ATL represents conceptual knowledge about objects [60], and integrates multiple features of an object [61]. In the present study, we identified a region in dorsal ATL showing pairwise MCD effects of faces and bodies, faces and scenes, and bodies and scenes. However, we did not find significant MCD effects in this region in the analysis with all four categories.

While ATL might represent conceptual knowledge integrating across multiple features [60, 61], representations of objects from different categories in this area might nonetheless be encoded by separate nearby regions, without one single area integrating all categories. In the case of patients with semantic dementia, multi-category deficits following ATL lesions could result from simultaneous damage to multiple category-selective regions. Indeed, the ATL is organized

into a complex topography of subregions with distinct connectivity profiles [62], and patients with semantic dementia are likely to have impairments to multiple subregions.

Alternatively, the lack of a significant voxels in ATL in the analysis with all four categories might be due to limitations in our study. Inspection of the results reveals subthreshold, bilateral MCD effects in the lateral ATL (Fig. 2), suggesting that studies with greater statistical power might be able to identify 4-way MCD effects in this region that survive correction for multiple comparisons. It is well established that fMRI data in the ATL are affected by susceptibility issues [63], and a larger amount of data might be needed to observe reliable results.

In addition to AG and ATL, we observed MCD effects in the left middle temporal gyrus (MTG) between artifacts and scenes, artifacts and bodies, and artifacts and faces. Unlike AG, this region did not show MCD effects in the analysis with all four categories. Left MTG has been previously implicated in the representation of artifacts [11, 64, 14]. In addition, overlap between responses to hands and tools has been reported in the vicinity of this area [65]. The findings in the present study suggest that left MTG might encode representations not only of artifacts in isolation, but also of their interactions with the human body, including the face (i.e. flatware, glasses, hats). MCD between some pairs of categories was also observed in a portion of ventral occipitotemporal cortex (Fig. 4). This observation converges with recent reports of a heteromodal semantic hub in the fusiform gyrus [66, 67] to suggest that some integration might already occur in posterior temporal cortex, but additional studies are needed to clarify the functional implications of this finding.

Besides AG and ATL, another brain region often implicated in semantic integration is the precuneus [51]. Indeed, a recent study used linguistic stimuli to study integration between words for objects from different categories, and found that precuneus - but not AG - shows stronger responses to sentences including the names of entities from multiple different categories than to sentences including only entities from a same category [22]. While in our study participants watched complex, quesi-naturalistic stimuli (as opposed to processing sentences), our results are consistent with and complementary to the findings by Rabini and colleagues [22]. The hypothesis that AG encodes complex spatiotemporal relations between entities predicts that it would integrate information across multiple categories when entities from different categories are present within a situation, but also when only entities from one category are present. In the study by Rabini and colleagues [22], both types of sentences described events featuring spatiotemporal interactions between multiple entities. Therefore, the hypothesized role of AG would not predict a difference in the overall amount of response between the two sentence types.

It is possible that precuneus might also contribute to multi-category information representation. In fact, we did find MCD effects in the precuneus when using two of the three artificial neural network architectures (i.e. the 1-Layer and the 5-Layer network, Supplementary Fig. S3). However, the MCD effects were not observed when using the 5-Layer densely connected architecture. Additional studies will be needed to test the robustness of MCD effects in the precuneus during the perception of complex dynamic videos, and to rule out that these effects are specific to language processing.

More work remains to be done to fully understand how information from multiple category-selective brain regions is encoded. In this study, we investigated multi-category dependence by searching for MCD sites whose responses are better predicted by the multivariate response patterns across multiple regions that respond preferentially to different categories, than by the response patterns in regions that are all selective for a same category. We identified a cortical map of brain regions whose responses are better predicted by the joint responses across multiple category-selective regions. However, several questions remain open. Additional research will be needed to investigate what kind of computations occur within these sites, and to determine whether they use information about objects from different categories to compute representations of their relationships and interactions. Furthermore, different MCD sites might support distinct cognitive functions. Finally, the methods used in this study are correlational: future investigations could evaluate the causal relationship between responses in category-selective regions and MCD sites using techniques such as combined TMS-fMRI.

In conclusion, we identified a region in the left AG whose responses are better predicted by the joint patterns of activity across multiple category-selective networks. This region is surrounded by a cortical map of areas showing MCD effects for specific pairs of object categories. In addition, we found evidence for multi-category dependence between some subsets of categories in the dorsal ATL and in left MTG. Together, these results show that multi-category information is not encoded in a single centralized site. Instead, multi-category dependence occurs in multiple cortical areas, which might in turn support distinct cognitive functions.

Acknowledgments

We would like to thank the researchers who contributed to the *studyforrest* project (Hanke et al., 2016; Sengupta et al., 2016) for sharing their data, and the developers of fmriprep (Esteban et al., 2018) for their assistance with the fmriprep

preprocessing pipeline. This work was supported by a startup grant from Boston College and by NSF grant 1943862 to Stefano Anzellotti.

References

[1] Kristen A Dunfield and Valerie A Kuhlmeier. Intention-mediated selective helping in infancy. *Psychological science*, 21(4):523–527, 2010.

[2] Angelina Cleroux and Ori Friedman. Young children infer feelings of ownership from habitual use. *Emotion*, 2020.

[3] Hz Hecaen and R Angelergues. Agnosia for faces (prosopagnosia). *Archives of neurology*, 7(2):92–100, 1962.

[4] Justine Sergent, Shinsuke Ohta, and BRENNAN MACDONALD. Functional neuroanatomy of face and object processing: a positron emission tomography study. *Brain*, 115(1):15–36, 1992.

[5] Nancy Kanwisher, Josh McDermott, and Marvin M Chun. The fusiform face area: a module in human extrastriate cortex specialized for face perception. *Journal of neuroscience*, 17(11):4302–4311, 1997.

[6] Russell Epstein and Nancy Kanwisher. A cortical representation of the local visual environment. *Nature*, 392(6676):598, 1998.

[7] Paul E Downing, Yuhong Jiang, Miles Shuman, and Nancy Kanwisher. A cortical area selective for visual processing of the human body. *Science*, 293(5539):2470–2473, 2001.

[8] Alex Martin and Linda L Chao. Semantic memory and the brain: structure and processes. *Current opinion in neurobiology*, 11(2):194–201, 2001.

[9] Aina Puce, Truett Allison, Maryam Asgari, John C Gore, and Gregory McCarthy. Differential sensitivity of human visual cortex to faces, letterstrings, and textures: a functional magnetic resonance imaging study. *Journal of neuroscience*, 16(16):5205–5215, 1996.

[10] Isabel Gauthier, Michael J Tarr, Jill Moylan, Pawel Skudlarski, John C Gore, and Adam W Anderson. The fusiform "face area" is part of a network that processes faces at the individual level. *Journal of cognitive neuroscience*, 12(3):495–504, 2000.

[11] Michael S Beauchamp, Kathryn E Lee, James V Haxby, and Alex Martin. Fmri responses to video and point-light displays of moving humans and manipulable objects. *Journal of cognitive neuroscience*, 15(7):991–1001, 2003.

[12] Rebecca F Schwarzlose, Chris I Baker, and Nancy Kanwisher. Separate face and body selectivity on the fusiform gyrus. *Journal of Neuroscience*, 25(47):11055–11059, 2005.

[13] Linda L Chao, James V Haxby, and Alex Martin. Attribute-based neural substrates in temporal cortex for perceiving and knowing about objects. *Nature neuroscience*, 2(10):913–919, 1999.

[14] Bradford Z Mahon, Shawn C Milleville, Gioia AL Negri, Raffaella I Rumiati, Alfonso Caramazza, and Alex Martin. Action-related properties shape object representations in the ventral stream. *Neuron*, 55(3):507–520, 2007.

[15] Russell A Epstein and Chris I Baker. Scene perception in the human brain. *Annual review of vision science*, 5:373–397, 2019.

[16] Karalyn Patterson, Peter J Nestor, and Timothy T Rogers. Where do you know what you know? the representation of semantic knowledge in the human brain. *Nature Reviews Neuroscience*, 8(12):976, 2007.

[17] Karalyn Patterson and Matthew A Lambon Ralph. The hub-and-spoke hypothesis of semantic memory. In *Neurobiology of language*, pages 765–775. Elsevier, 2016.

[18] Matthew A Lambon Ralph, Elizabeth Jefferies, Karalyn Patterson, and Timothy T Rogers. The neural and computational bases of semantic cognition. *Nature Reviews Neuroscience*, 18(1):42, 2017.

[19] John R Hodges, Karalyn Patterson, Susan Oxbury, and Elaine Funnell. Semantic dementia: Progressive fluent aphasia with temporal lobe atrophy. *Brain*, 115(6):1783–1806, 1992.

[20] Gorana Pobric, Elizabeth Jefferies, and Matthew A Lambon Ralph. Category-specific versus category-general semantic impairment induced by transcranial magnetic stimulation. *Current biology*, 20(10):964–968, 2010.

[21] Amy Rose Price, Jonathan E Peelle, Michael F Bonner, Murray Grossman, and Roy H Hamilton. Causal evidence for a mechanism of semantic integration in the angular gyrus as revealed by high-definition transcranial direct current stimulation. *Journal of Neuroscience*, 36(13):3829–3838, 2016.

[22] Giuseppe Rabini, Silvia Ubaldi, and Scott L Fairhall. Combining concepts across categorical domains: a linking role of the precuneus. *Neurobiology of Language*, pages 1–50, 2021.

[23] Michael Hanke, Nico Adelhöfer, Daniel Kottke, Vittorio Iacovella, Ayan Sengupta, Falko R Kaule, Roland Nigbur, Alexander Q Waite, Florian Baumgartner, and Jörg Stadler. A studyforrest extension, simultaneous fmri and eye gaze recordings during prolonged natural stimulation. *Scientific data*, 3:160092, 2016.

[24] Stefano Anzellotti, Alfonso Caramazza, and Rebecca Saxe. Multivariate pattern dependence. *PLoS computational biology*, 13(11):e1005799, 2017.

[25] Stefano Anzellotti and Marc N Coutanche. Beyond functional connectivity: investigating networks of multivariate representations. *Trends in cognitive sciences*, 22(3):258–269, 2018.

[26] Mengting Fang, Craig Poskanzer, and Stefano Anzellotti. Pymvpd: A toolbox for multivariate pattern dependence. *Frontiers in Neuroinformatics*, 16, 2022.

[27] Yashar Behzadi, Khaled Restom, Joy Liau, and Thomas T Liu. A component based noise correction method (compcor) for bold and perfusion based fmri. *Neuroimage*, 37(1):90–101, 2007.

[28] Mark W Woolrich, Brian D Ripley, Michael Brady, and Stephen M Smith. Temporal autocorrelation in univariate linear modeling of fmri data. *Neuroimage*, 14(6):1370–1386, 2001.

[29] James V. Haxby, Maria Gobbini, Maura Furey, Alumit Ishai, Jennifer L. Schouten, and Pietro Pietrini. Distributed and overlapping representations of faces and objects in ventral temporal cortex. *Science (New York, N.Y.)*, 293:2425–30, 10 2001.

[30] Kenneth A Norman, Sean Polyn, Greg Detre, and James V Haxby. Beyond mind-reading: Multi-voxel pattern analysis of fmri data. *Trends in cognitive sciences*, 10:424–30, 10 2006.

[31] Nikolaus Kriegeskorte, Elia Formisano, Bettina Sorger, and Rainer Goebel. Individual faces elicit distinct response patterns in human anterior temporal cortex. *Proceedings of the National Academy of Sciences*, 104(51):20600–20605, 2007.

[32] Adrian Nestor, David C Plaut, and Marlene Behrmann. Unraveling the distributed neural code of facial identity through spatiotemporal pattern analysis. *Proceedings of the National Academy of Sciences*, 108(24):9998–10003, 2011.

[33] Stefano Anzellotti, Scott L Fairhall, and Alfonso Caramazza. Decoding representations of face identity that are tolerant to rotation. *Cerebral Cortex*, 24(8):1988–1995, 2013.

[34] Chun Siong Soon, Marcel Brass, Hans-Jochen Heinze, and John-Dylan Haynes. Unconscious determinants of free decisions in the human brain. *Nature neuroscience*, 11(5):543, 2008.

[35] Jorie Koster-Hale, Rebecca Saxe, James Dungan, and Liane L Young. Decoding moral judgments from neural representations of intentions. *Proceedings of the National Academy of Sciences*, 110(14):5648–5653, 2013.

[36] Stefano Anzellotti, Evelina Fedorenko, Alexander JE Kell, Alfonso Caramazza, and Rebecca Saxe. Measuring and modeling nonlinear interactions between brain regions with fmri. *bioRxiv*, page 074856, 2017.

[37] Colin Fyfe. A neural network for pca and beyond. *Neural Processing Letters*, 6(1-2):33–41, 1997.

[38] Marius V Peelen, Alison J Wiggett, and Paul E Downing. Patterns of fmri activity dissociate overlapping functional brain areas that respond to biological motion. *Neuron*, 49(6):815–822, 2006.

[39] Craig Poskanzer, Mengting Fang, Aidas Aglinskas, and Stefano Anzellotti. Controlling for spurious nonlinear dependence in connectivity analyses. *Neuroinformatics*, pages 1–13, 2021.

[40] Hrushikesh Mhaskar, Qianli Liao, and Tomaso Poggio. When and why are deep networks better than shallow ones? In *Thirty-First AAAI Conference on Artificial Intelligence*, 2017.

[41] Sepp Hochreiter. The vanishing gradient problem during learning recurrent neural nets and problem solutions. *International Journal of Uncertainty, Fuzziness and Knowledge-Based Systems*, 6(02):107–116, 1998.

[42] Gao Huang, Zhuang Liu, Laurens Van Der Maaten, and Kilian Q Weinberger. Densely connected convolutional networks. In *Proceedings of the IEEE conference on computer vision and pattern recognition*, pages 4700–4708, 2017.

[43] Nikolaus Kriegeskorte, Marieke Mur, and Peter A Bandettini. Representational similarity analysis-connecting the branches of systems neuroscience. *Frontiers in systems neuroscience*, 2:4, 2008.

[44] Jörn Diedrichsen and Nikolaus Kriegeskorte. Representational models: A common framework for understanding encoding, pattern-component, and representational-similarity analysis. *PLoS computational biology*, 13(4):e1005508, 2017.

[45] Karl J. Friston, Jörn Diedrichsen, Emma Holmes, and Peter Zeidman. Variational representational similarity analysis. *NeuroImage*, 201:115986, 2019.

[46] T Yarkoni, RA Poldrack, TE Nichols, DC Van Essen, and TD Wager. Neurosynth: a new platform for largescale automated synthesis of human functional neuroimaging data. front neuroinformatics conf abstr 4th incf congr neuroinformatics. 2011.

[47] Heidi M Bonnici, Franziska R Richter, Yasemin Yazar, and Jon S Simons. Multimodal feature integration in the angular gyrus during episodic and semantic retrieval. *Journal of Neuroscience*, 36(20):5462–5471, 2016.

[48] Nikolaus Kriegeskorte, Marieke Mur, Douglas A Ruff, Roozbeh Kiani, Jerzy Bodurka, Hossein Esteky, Keiji Tanaka, and Peter A Bandettini. Matching categorical object representations in inferior temporal cortex of man and monkey. *Neuron*, 60(6):1126–1141, 2008.

[49] Stefania Bracci, J Brendan Ritchie, Ioannis Kalfas, and Hans P Op de Beeck. The ventral visual pathway represents animal appearance over animacy, unlike human behavior and deep neural networks. *Journal of Neuroscience*, 39(33):6513–6525, 2019.

[50] Norman Geschwind. Language and the brain. *Scientific American*, 226(4):76–83, 1972.

[51] Jeffrey R Binder, Rutvik H Desai, William W Graves, and Lisa L Conant. Where is the semantic system? a critical review and meta-analysis of 120 functional neuroimaging studies. *Cerebral Cortex*, 19(12):2767–2796, 2009.

[52] Anthony D Wagner, Benjamin J Shannon, Itamar Kahn, and Randy L Buckner. Parietal lobe contributions to episodic memory retrieval. *Trends in cognitive sciences*, 9(9):445–453, 2005.

[53] Marian E Berryhill, Lisa Phuong, Lauren Picasso, Roberto Cabeza, and Ingrid R Olson. Parietal lobe and episodic memory: bilateral damage causes impaired free recall of autobiographical memory. *Journal of Neuroscience*, 27(52):14415–14423, 2007.

[54] Maurizio Corbetta and Gordon L Shulman. Control of goal-directed and stimulus-driven attention in the brain. *Nature reviews neuroscience*, 3(3):201–215, 2002.

[55] Jeffrey R Binder and Rutvik H Desai. The neurobiology of semantic memory. *Trends in cognitive sciences*, 15(11):527–536, 2011.

[56] Isabella C Wagner, Mariët van Buuren, Marijn CW Kroes, Tjerk P Gutteling, Marieke van der Linden, Richard G Morris, and Guillén Fernández. Schematic memory components converge within angular gyrus during retrieval. *Elife*, 4:e09668, 2015.

[57] Gina F Humphreys, Matthew A Lambon Ralph, and Jon S Simons. A unifying account of angular gyrus contributions to episodic and semantic cognition. *Trends in Neurosciences*, 2021.

[58] Amy R Price, Michael F Bonner, Jonathan E Peelle, and Murray Grossman. Converging evidence for the neuroanatomic basis of combinatorial semantics in the angular gyrus. *Journal of Neuroscience*, 35(7):3276–3284, 2015.

[59] Lucilla Lanzoni, Daniela Ravasio, Hannah Thompson, Deniz Vatansever, Daniel Margulies, Jonathan Smallwood, and Elizabeth Jefferies. The role of default mode network in semantic cue integration. *Neuroimage*, 219:117019, 2020.

[60] Marius V Peelen and Alfonso Caramazza. Conceptual object representations in human anterior temporal cortex. *Journal of Neuroscience*, 32(45):15728–15736, 2012.

[61] Marc N Coutanche and Sharon L Thompson-Schill. Creating concepts from converging features in human cortex. *Cerebral cortex*, 25(9):2584–2593, 2015.

[62] Andrew S Persichetti, Joseph M Denning, Stephen J Gotts, and Alex Martin. A data-driven functional mapping of the anterior temporal lobes. *Journal of Neuroscience*, 2021.

[63] Joseph T Devlin, Richard P Russell, Matt H Davis, Cathy J Price, James Wilson, Helen E Moss, Paul M Matthews, and Lorraine K Tyler. Susceptibility-induced loss of signal: comparing pet and fmri on a semantic task. *Neuroimage*, 11(6):589–600, 2000.

[64] Michael S Beauchamp and Alex Martin. Grounding object concepts in perception and action: evidence from fmri studies of tools. *Cortex*, 43(3):461–468, 2007.

[65] Stefania Bracci, Cristiana Cavina-Pratesi, Magdalena Ietswaart, Alfonso Caramazza, and Marius V Peelen. Closely overlapping responses to tools and hands in left lateral occipitotemporal cortex. *Journal of neurophysiology*, 107(5):1443–1456, 2012.

[66] Kiefer James Forseth, Cihan Mehmet Kadipasaoglu, Christopher Richard Conner, Gregory Hickok, Robert Thomas Knight, and Nitin Tandon. A lexical semantic hub for heteromodal naming in middle fusiform gyrus. *Brain*, 141(7):2112–2126, 2018.

[67] Lang Qin, Bingjiang Lyu, Su Shu, Yayan Yin, Xiongfei Wang, Jianqiao Ge, Wai-Ting Siok, and Jia-Hong Gao. A heteromodal word-meaning binding site in the visual word form area under top-down frontoparietal control. *Journal of Neuroscience*, 41(17):3854–3869, 2021.

Supplementary Materials

Supplementary Figures and Tables

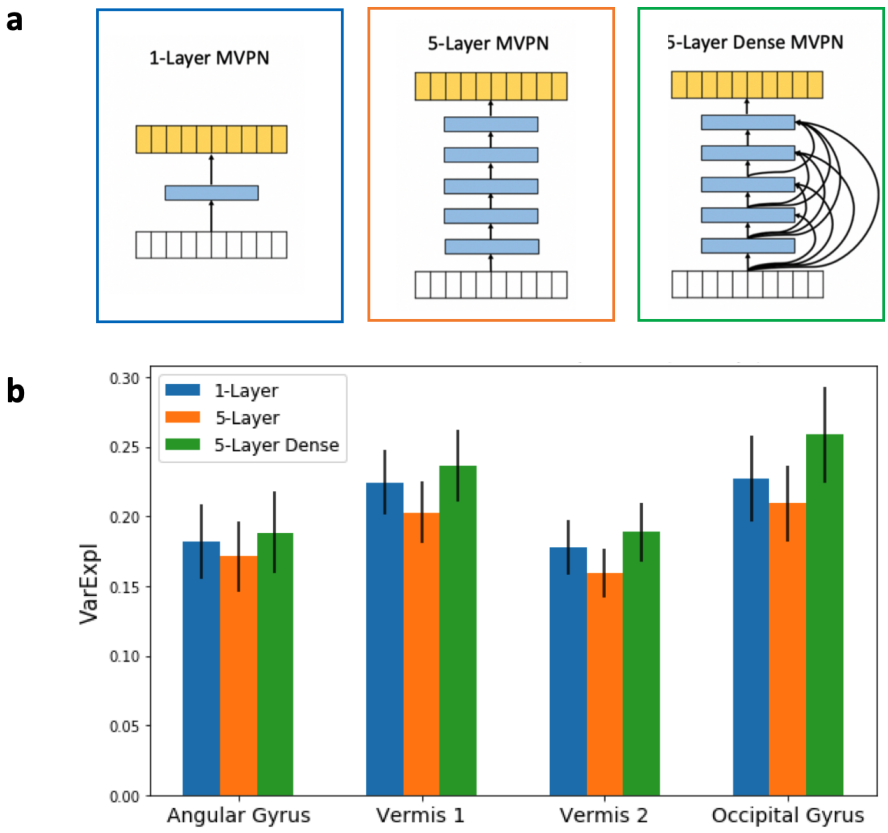

Figure S1: **a.** Different MVPN model architectures. 1-Layer MVPN (left): 1-layer fully-connected linear neural network model; 5-Layer MVPN (middle): 5-layer fully-connected linear neural network model; 5-Layer Dense MVPN (right): 5-layer fully-connected linear neural network model with dense connections. **b.** Different predictive accuracy of MVPN models across candidate MCD sites and network architectures by the combination of response patterns from all category-selective regions. Error bars indicate the standard error of the mean (SEM).

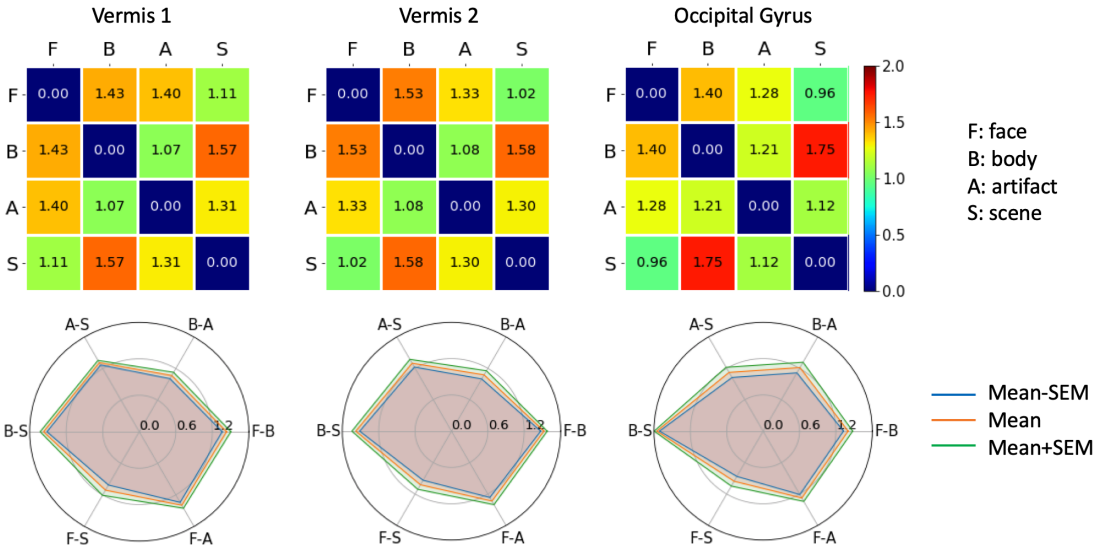

Figure S2: RDMs (top) and radar charts (bottom) for average brain activities across subjects in vermis 1, vermis 2, and occipital gyrus. The three regions were first identified as candidate MCD sites by the combined-minus-max analysis but were then excluded by the control analysis. In each radar chart, the middle boundary represents the average representational dissimilarity across subjects, the inner boundary represents the average representational dissimilarity minus the standard error of the mean (SEM), and the outer boundary represents the average representational dissimilarity plus SEM.

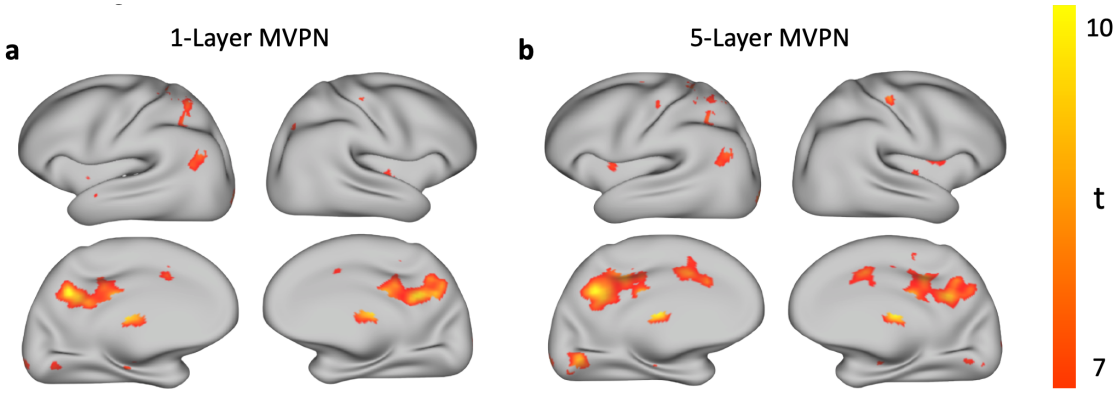

Figure S3: **a.** Statistical t-maps of the 1-Layer MVPN model computed from Δ varExpl across subjects. **b.** Statistical t-maps of the 5-Layer MVPN model computed from Δ varExpl across subjects. Δ varExpl is the voxelwise difference between the variance explained predicted by the combined model using all category-selective regions as input, and the variance explained predicted by the model using regions selective for the single best-predicting category. The SnPM thresholds corrected at $p < 0.05$ FWE are 4.78 (1-Layer MVPN) and 4.69 (5-Layer MVPN).T-maps are thresholded within the range [7,10] for visualization purposes.